AGU PUBLICATIONS

JGR

Journal of Geophysical Research: Space Physics

BRIEF REPORT

10.1002/2013JA018870

Key Points:
- The Andes Mountains favor the ionospheric wave activity at the eastern side
- This feature agrees with some dynamical aspects of the lower atmosphere

Correspondence to:
A. de la Torre,
adelatorre@austral.edu.ar

Citation:
de la Torre, A., P. Alexander, P. Llamedo, R. Hierro, B. Nava, S. Radicella, T. Schmidt, and J. Wickert (2014), Wave activity at ionospheric heights above the Andes Mountains detected from FORMOSAT-3/COSMIC GPS radio occultation data, *J. Geophys. Res. Space Physics*, *119*, doi:10.1002/2013JA018870.

Received 16 MAR 2013
Accepted 21 JAN 2014
Accepted article online 27 JAN 2014

Wave activity at ionospheric heights above the Andes Mountains detected from FORMOSAT-3/COSMIC GPS radio occultation data

A. de la Torre[1], P. Alexander[2], P. Llamedo[1], R. Hierro[1], B. Nava[3], S. Radicella[3], T. Schmidt[4], and J. Wickert[4]

[1]Facultad de Ingeniería, Universidad Austral and CONICET, Buenos Aires, Argentina, [2]Departamento de Física, Facultad de Ciencias Exactas y Naturales, Universidad de Buenos Aires and CONICET, Buenos Aires, Argentina, [3]Telecommunications/ICT for Development Laboratory, The Abdus Salam International Centre for Theoretical Physics, Trieste, Italy, [4]Helmholtz Centre Potsdam, GFZ German Research Centre for Geosciences, Potsdam, Germany

Abstract An estimation of the ionospheric wave activity, derived from 4 years of FORMOSAT-3/ COSMIC GPS (Taiwan's Formosa Satellite Mission 3/Constellation Observing System for Meteorology—Global Positioning System) radio occultation electron density data, is presented. A systematic enhancement at the eastern side of the Andes range with respect to the western side is observed. A fitting method to remove the wavelike component from each measured profile and estimate the wave activity is described. The differential effect introduced by the action of orography on the generation, to the eastern side of the Andes, of mountain waves, deep convection waves, or even secondary waves aloft after momentum deposition in the middle atmosphere, is suggested.

1. Introduction

Internal atmospheric gravity waves (GWs) in the neutral atmosphere and their ionospheric evidence as traveling ionospheric disturbances (TIDs) have been studied in depth through a wide range of experiments, modeling, and theoretical efforts since *Hines* [1960]. Several comprehensive papers and books followed Hines' work [e.g., *Testud*, 1972; *Yeh and Liu*, 1974; *Gossard and Hooke*, 1975] and more recently, as described in a review by *Fritts and Lund* [2011, and references therein] (FL11). FL11 points out the observational evidence and persistence of GWs, extending to very high ionospheric altitudes and defining representative GW scales and frequencies as functions of altitude. These features suggest sources of GWs ranging from deep convection at tropical latitudes to aurora at high latitudes. There is general agreement in that the primary GW sources occur in the lower neutral atmosphere under calm thermospheric-ionospheric conditions and GW vertical wavelengths and periods increase monotonically with height at ionospheric altitudes [*Oliver et al*., 1997].

It is assumed that TIDs are ionospheric manifestations of GWs, with the ionosphere acting as a passive tracer to display manifestation of the motion of the neutral atmosphere [*Francis*, 1975]. Observations of electron density and minor constituent fluctuations may be detected by various instruments like incoherent scatter radar, ionosondes, all-sky airglow imagers, Global Positioning System (GPS) receivers, on site measurements, and satellite remote sensing [e.g., *Nicolls et al*., 2004; *Brunini et al*., 2004; *Miró Amarante et al*., 2004; *Martinis et al*., 2006; *Earle et al*., 2008; *Wickert et al*., 2009; *Scheer and Reisin*, 2010]. Near the Andes, at the El Leoncito Observatory (Argentina) (31.8°S, 69.3°W) where the main sources of GWs in the lower and middle atmosphere are found [*Fritts and Alexander*, 2003], *Smith et al*. [2009] reported for the first time imaging observations of stationary mesospheric gravity waves in the nightglow emissions of OH, from all-sky images. Wave features with zero or near-zero horizontal phase speed and lifetimes of several hours, in addition to wind direction as well as the orientation of the waves relative to the mountains, suggested that these were mountain waves (MWs) generated at tropospheric heights.

GPS radio occultation (RO) is a well-known remote sensing technique used for measuring the physical properties of planetary atmospheres [e.g., *Melbourne et al*., 1994]. It relies on the detection of a change in a radio signal as it passes through the planet's atmosphere, i.e., as it is occulted by the atmosphere. When electromagnetic radiation passes through the atmosphere, it is refracted. The magnitude of the refraction depends on the gradient of refractivity normal to the path, which in turn depends on the gradients of density

and the water vapor content. The effect is most pronounced when the radiation traverses a long atmospheric limb path. At radio frequencies, the amount of bending cannot be measured directly; instead, the bending can be calculated using the Doppler shift of the signal given the geometry of the emitter and receiver. The amount of bending can be related to the refractive index by using an Abel transform. In the case of the neutral atmosphere, information on temperature (T), pressure, and water vapor content can be derived. The GPS signals can be received on low Earth orbit (LEO) satellites. The GPS limb sounding technique has proved to be a powerful tool for remote sensing of the Earth's ionosphere [e.g., *Kursinski et al*., 1997; *Hajj and Romans*, 1998]. LEO missions such as CHAMP and Satélite de Aplicaciones Científicas-C carried a dual frequency GPS receiver on board and offered a new chance for improving measuring techniques and algorithms for retrieving the electron density (N_e), monitoring the actual state of the global ionosphere on a continuous basis. Radio occultation measurements of GPS carrier phases on board a LEO satellite like CHAMP enabled the computation of the vertical refractivity profile from the LEO satellite orbit height down to the Earth's surface. Since the index of refractivity of the ionosphere depends mainly on the number of free electrons, the inversion of the measured signals provided the vertical electron density profile [e.g., *Jakowski et al*., 2002]. Until now, the GPS RO missions CHAMP [*Wickert et al*., 2009], Gravity Recovery and Climate Experiment, and FORMOSAT-3/COSMIC [*Anthes et al*., 2008] provide a total of roughly 3000 globally distributed measurements per day. *Arras et al*. [2008] pointed out that small-scale ionospheric irregularities, like sporadic *E* layers, may be analyzed from GPS RO data, represented by vertical profiles of signal-to-noise ratio, phase differences, or ionospheric excess phases. Near the region considered by *Smith et al*. [2009], above the El Leoncito Observatory close to the highest Andes tops (31.8°S, 69.3°W), *de la Torre and Alexander* [2005] and *de la Torre et al*. [2006] have discussed possible sources and vertical propagation of large amplitude MW events from RO neutral temperature data. From mesoscale simulations, *de la Torre et al*. [2012] showed representative large amplitude GW events during winter at tropospheric heights, with considerable enhanced wave activity to the eastern side of the Andes. In section 2, we show indications of wave activity at ionospheric heights above the highest Andes Mountains from RO data. The possible relationship to MW forcing is discussed. In section 3, some conclusions are drawn and further work in progress is outlined.

2. Wave Activity in the Ionosphere Above the Andes

The present study uses the latest postprocessed data (product version 2010.2640) from the COSMIC mission provided by CDAAC (COSMIC Data Analysis and Archive Center-http://cdaac-www.cosmic.ucar.edu/cdaac/index.html-). We considered all GPS RO events observed between 1 January 2007 and 31 December 2010. This period corresponds to the last minimum in solar cycle variability. Nevertheless, we do not expect variations in solar activity to modify the main results described here. We considered the region limited, at ground level, by latitudes 30–36°S and longitudes 65–75°W (Figure 1a). The highest Andes tops may be found in this region between longitudes 69.5°W and 70.5°W. A total of 1604 occultation events (484, 400, 435, and 285 N_e annual vertical profiles, in fact, "slanted" lines of tangent points (LTP) from 2007, 2008, 2009, and 2010, respectively) were retrieved. Their lowest levels fit within the region mentioned above. Before and after this period, a considerably lower number of profiles were available. MWs in the lower and middle atmosphere are expected to occur above the eastern side of this band as the result of forcing by the westerly winds. The largest MW amplitudes are generally present during winter [e.g., *de la Torre et al*., 2012]; however, during late spring, summer and early fall, considerable amplitudes, sometimes capable of triggering deep convection events, have been also identified [e.g., *de la Torre et al*., 1996; *Hierro et al*., 2013]. We analyze the possibility that GWs of topographic origin or even secondary waves generated by the breaking of these waves could produce a systematic observable wave activity also in the lower thermosphere, enhanced to the eastern side of this band as compared to the western side. In addition to MWs, GWs from deep convection origin can reach nonlinear amplitudes and break or reach critical levels in the stratosphere-mesosphere-thermosphere as well where they are finally expected to be dissipated from molecular viscosity [*Vadas*, 2013]. Severe deep convection events frequently detected to the eastern side of the Andes Range at midlatitudes could provide a significant contribution to the overall wave activity, mainly during summer [*Hierro et al*., 2013].

In Figure 1b, altitude-longitude LTP projections corresponding to the first 200 RO events detected during 2007 are shown to illustrate typical paths sounded from lower troposphere to ionospheric heights. Red and blue squares encompass representative altitude (110–200 km) and longitude (65–75°W) sectors, selected to estimate wave activity above the eastern and western sides of the highest Andes Mountain tops. This "tops"

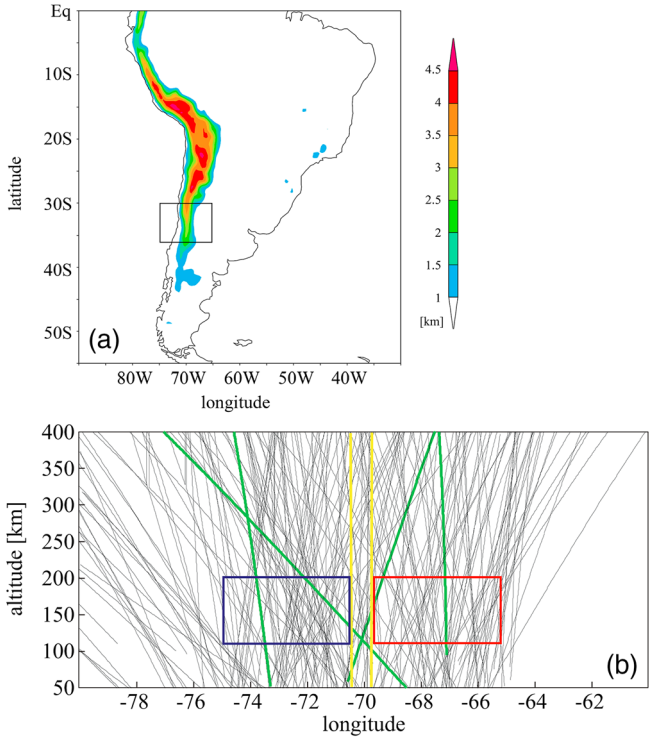

Figure 1. (a) The considered region, limited at ground level, by latitudes 30–36°S and longitudes 65–75°W. The highest Andes tops may be roughly isolated in that region inside a meridional band defined by longitudes 69.5°W and 70.5°W. (b) An example of altitude-longitude LTP projections, corresponding to the first 200 RO events during 2007, as detected at ground level between 30–36°S and 65–75°W. Red and blue squares respectively encompass the altitude and longitude intervals selected to estimate possible wave activity, above the eastern and western sides of the highest Andes tops. This tops area is defined by the two vertical yellow fringes. Four different LTPs are represented by green highlighted curves: sounding the eastern (or western) Andes side at the ionosphere and simultaneously sounding the eastern (or western) side at the troposphere.

area is indicated by the two vertical yellow fringes. The natural slanted character of LTPs allows for different paths of the GPS radio waves, illustrated by green highlighted curves in the figure. Our intention here is only to compare wave activity on both ionospheric sides from measured RO N_e profiles, without endeavoring to reach any definitive conclusions about the origin of the observed perturbations. In doing so, we considered two possible proxies: the mean relative N_e variance content (MRVC) from a total of M profiles

$$\mathrm{MRVC} = \frac{1}{M}\sum_{k=1}^{M}\frac{1}{z_2 - z_1}\int_{z_1}^{z_2}\left(\frac{\delta N_{e_k}}{N_{e_k}}\right)^2 \mathrm{d}z, \tag{1}$$

where z_1 and z_2 are the lower and upper limits of integration and $\delta N_{ek} = N_{ek} - \overline{N_{ek}}$ is the difference between each measured and background k profile. Instead, we may consider the mean absolute variance content

$$\mathrm{MAVC} = \frac{1}{M}\sum_{k=1}^{M}\frac{1}{z_2 - z_1}\int_{z_1}^{z_2}(\delta N_{e_k})^2 \mathrm{d}z. \tag{2}$$

Similar to the calculation of wave activity from neutral temperature profiles in the lower and middle atmosphere, (1) would seem appropriate, as long as it takes into account the altitude variation (usually an increase) of N_e across the E region, weighting the relative importance of the perturbation component with respect to the background profile. Nevertheless [e.g., *Tsai et al.*, 2001], retrieved profiles from RO data frequently depict negative or positive bias or even negative N_e values below altitudes around 100 km. These errors are due to (1) the considerable spatial extension of the averaging in the retrieval process around the tangent point at ionospheric heights (≈ 1000 km) and (2) the spherical inhomogeneity of N_e, expected at low and midlatitude regions (in the lower neutral atmosphere the averaging around the tangent point in the T retrieval process is considerably lower). Below approximately 100 km altitude, the plasma density is usually quite lower than in the F region. Data obtained from RO measurements represent an integral of the plasma density along the raypath of the radio wave. At the tangential point at lower altitudes, the plasma density may be contaminated by the plasma density in the F region at different locations. Moreover, possible sporadic E layers, which appear around 100 km altitude, could also contaminate the results obtained in this study. From these arguments, we then estimate wave activity from (2), excluding lower altitude data and computing mean absolute variance content (MAVC) with z_1 and z_2 equal to 110 and 200 km, respectively. In order to estimate and compare the wave activity between the eastern and western sides of the Andes Range, the perturbation component extracted from each available profile was obtained after fitting polynomials with different 7°, here selected from 4° to 10°. Other possible fitting methods such as band-pass filters were not used here, because at this stage, we do not intend to provide a direct control or estimation of filtered wavelengths or wavelength ranges [*Schmidt et al.*, 2008]. On the other hand, the possibility of estimating vertical wavelengths is discarded, given the considerable differences that should be expected between "apparent" and "actual" vertical wavelengths retrieved from

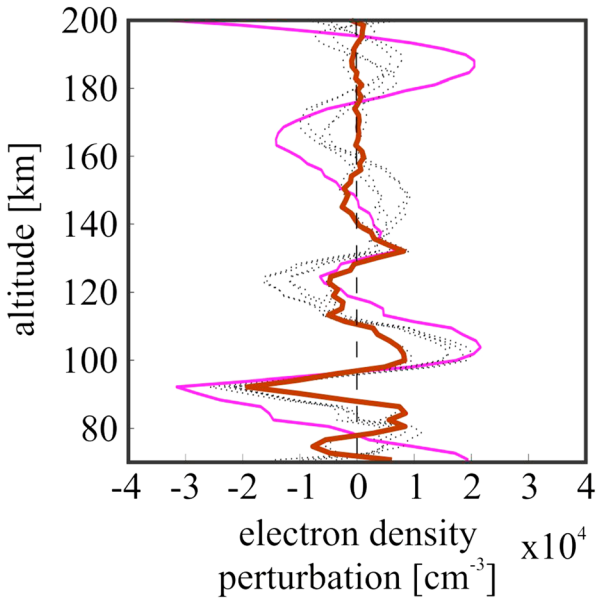

Figure 2. From a single illustrative "eastern" N_e vertical profile, seven progressive δN_e profiles were obtained after seven polynomial fittings and background subtraction. The profiles corresponding to the fourth (pink) and tenth degree (brown) are highlighted.

nonvertical (limb) soundings [*de la Torre and Alexander*, 1995], as it happens in the particular case of GPS RO data [*de la Torre and Alexander*, 2005]. This limitation is not present from nadir soundings or even from modeling simulations [e.g., *Miyoshi and Fujiwara*, 2009].

We inspected every N_e profile, and those exhibiting negative values or truncated segments of missing points were discarded. Figure 2 shows an illustrative "eastern" δN_e profile, obtained after the seven polynomial fittings (PF) and background subtraction processes. The expected progressive decreasing overall amplitude from fourth (pink) to tenth degree (brown) PF can be observed. To identify a criterion about the eastern or western location of the ionospheric segment of each profile, we established the longitude intersecting each LTP at the 100 km altitude. In Figure 3, MAVC corresponding to years 2007 to 2010 at western and eastern sides and for each PF degree is comparatively shown. A general qualitative enhancement in the eastern ionospheric wave activity may be observed. Applying (2) instead of (1), we do not take into account the weighting of each perturbation profile provided by N_e^{-1}, that would result in a smaller contribution of upper altitude perturbations with respect to the lower (because of the increase of N_e with altitude throughout 110–200 km). Although differences in wave activity between eastern and western ionospheric sectors are, as expected, not so large, a clear trend is established for every year and PF degree. The results shown in Figures 3a–3d have been tested as statistically significant. These are resistant to variations in the widening of fringes including the Andes tops and the altitude/latitude/longitude sector considered as well. We tried to further analyze the seasonal variability of these results, as we know from previous works (mainly from the last decade) that the largest mountain wave activity is expected during winter in the Southern Hemisphere, in coincidence with the variability of the subtropical jet stream and the tropospheric stability. Here we found an obstacle: we selected only a region close enough to the

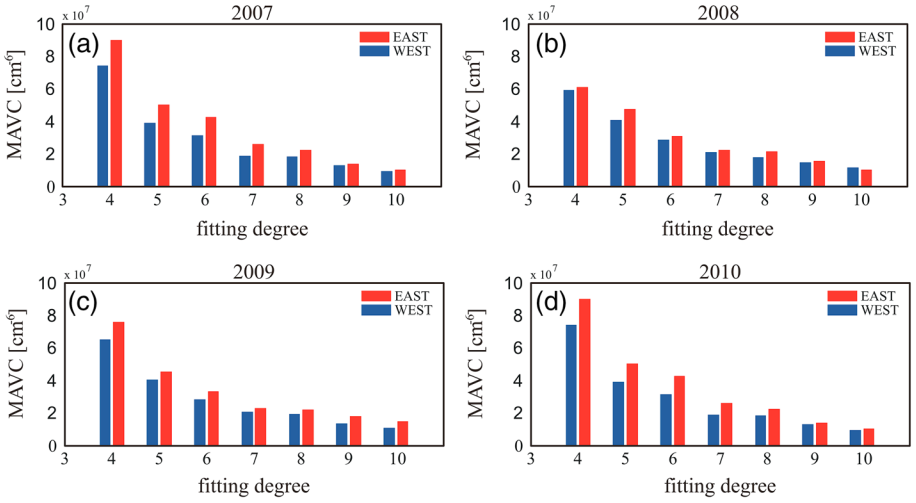

Figure 3. Electron density mean absolute variance content (MAVC), for the altitude/latitude/longitude selection: 110–200km/30–36°S/65–75°W, corresponding to the available FORMOSAT-3/COSMIC GPS RO events at both sides of the selected Andes Range region during (a) 2007 to (d) 2010, respectively.

highest Andes Range (30–36°S) to mainly take into account the possible orographic influence, as this gravity wave source by far is prevalent there. At the same time, we intended to avoid the inclusion of events located zonally too far away from the mountains, to guarantee a major isolation from other possible sources well above the ocean and the plains in the Argentinean region (65–70°W). As stated above, within this selected area, an average number of around 400 radio occultation events per year are available from COSMIC data. After discarding profiles exhibiting (i) negative biases and/or (ii) sporadic *E* behaviors or (iii) lying strictly above the "tops" area (as indicated by the two vertical yellow fringes in Figure 1), the remaining number of considered profiles per year at each side of the mountains is considerably reduced. To ensure the statistical significance of the results shown in Figure 3, we were constrained to avoid a seasonal stratification of the results, as this would have additionally reduced each set of remaining profiles by a 0.25 factor.

3. Discussion

We observed a larger intensity in electron density perturbations at the eastern side with respect to the western side of the Andes Range. As there are many ways to attempt this, we selected a polynomial fitting. We extracted the amplitude perturbation component from electron density vertical profiles and the filtering process is performed by seven different polynomial degrees. We do not know which polynomial degree performs better, but all of them lead to the same conclusion: there is a higher activity on the eastern side (but we cannot quantify in detail the difference with respect to the western side). We do not intend to use these results to draw conclusions regarding the origin of the larger intensity. The influence of the mountains at the eastern side and at the considered latitude bounds seems to be present, mainly through MW generation in winter and, possibly, GWs generated by severe and frequent deep convection processes in summer. These GWs may be able to reach considerable altitudes before breaking or finding critical levels or dissipating in the lower thermosphere. From these data, it is not possible to gain further insight on whether the main contribution to wave activity detected at ionospheric altitudes is due to primary waves or to radiation of secondary waves, after momentum deposition. The preliminary trends detected through MAVC may be supported by additional neutral wind information and possible critical level deposition at mesospheric regions (e.g., Sounding of the Atmosphere using Broadband Emission Radiometry data) as well as a wave activity correlation between the ionosphere and lower thermosphere, considering the RO profiles individually. Regarding the possible penetration of tropospheric waves, not necessarily larger amplitude waves are expected to produce larger effects at ionospheric heights. From mesoscale modeling results, single events of large amplitude MWs near the Andes are found to enhance wave activity to the eastern side and to transfer momentum flux to the background atmosphere at relatively low stratospheric heights [*de la Torre et al.*, 2012]. Small/moderate amplitude GWs could be more likely to reach saturation and breaking levels at higher altitudes.

Acknowledgments

This paper was prepared under grant CONICET PIP 0649. A. de la Torre, P. Alexander, and P. Llamedo are members of and R. Hierro holds a fellowship from CONICET. We acknowledge COSMIC data provided by UCAR and the data center CDAAC (http://cdaac-www.cosmic.ucar.edu/cdaac/index.html).

Robert Lysak thanks Richard A. Anthes, Yuichi Otsuka, and two anonymous reviewers for their assistance in evaluating this paper.

References

Anthes, R. A., et al. (2008), The COSMIC/FORMOSAT-3 Mission: Early results, *Bull. Am. Meteorol. Soc.*, *89*(3), 313–333, doi:10.1175/BAMS-89-3-313.

Arras, C., J. Wickert, C. Jacobi, S. Heise, G. Beyerle, and T. Schmidt (2008), A global climatology of ionospheric irregularities derived from GPS radio occultation, *Geophys. Res. Lett.*, *35*, L14809, doi:10.1029/2008GL034158.

Brunini, C., A. Meza, F. Azpilicueta, M. A. Van Zele, M. Gende, and A. Díaz (2004), A new ionospheric monitoring technology based on GPS, *Astrophys. Space Sci.*, *290*, 415–429.

de la Torre, A., and P. Alexander (1995), The interpretation of wavelengths and periods as measured from atmospheric balloons, *J. Appl. Meteorol.*, *34*, 2747–2756.

de la Torre, A., and P. Alexander (2005), Gravity waves above Andes detected from GPS radio occultation temperature profiles: Mountain forcing?, *Geophys. Res. Lett.*, *32*, L17815, doi:10.1029/2005GL022959.

de la Torre, A., H. Teitelbaum, and F. Vial (1996), Tropospheric and stratospheric wave measurements near the Andes Mountains, *J. Atmos. Terr. Phys.*, *58*, 521–530.

de la Torre, A., P. Alexander, P. Llamedo, C. Menéndez, T. Schmidt, and J. Wickert (2006), Gravity waves above the Andes detected from GPS radio occultation temperature profiles: Jet mechanism?, *Geophys. Res. Lett.*, *33*, L24810, doi:10.1029/2006GL027343.

de la Torre, A., P. Alexander, R. Hierro, P. Llamedo, A. Rolla, T. Schmidt, and J. Wickert (2012), Large-amplitude gravity waves above the southern Andes, the Drake Passage, and the Antarctic Peninsula, *J. Geophys. Res.*, *117*, D02106, doi:10.1029/2011JD016377.

Earle, G. D., A. M. Musumba, and S. L. Vadas (2008), Satellite-based measurements of gravity wave-induced midlatitude plasma density perturbations, *J. Geophys. Res.*, *113*, A03303, doi:10.1029/2007JA012766.

Francis, S. H. (1975), Global propagation of atmospheric gravity waves: A review, *J. Atmos. Terr. Phys.*, *11*, 571–594.

Fritts, D. C., and J. Alexander (2003), Gravity wave dynamics and effects in the middle atmosphere, *Rev. Geophys.*, *41*(1), 1003, doi:10.1029/2001RG000106.

Fritts, D. C., and T. Lund (2011), Gravity wave influences in the thermosphere and ionosphere: Observations and recent modeling, in *Aeronomy of the Earth's Atmosphere and Ionosphere*, edited by M. A. Abdu, D. Pancheva, and A. Bhattacharyya, pp. 109–130, Springer, New York.

Gossard, E. E., and W. H. Hooke (1975), *Waves in the Atmosphere*, Elsevier, New York.

Hajj, G. A., and L. J. Romans (1998), Ionospheric electron density profiles obtained with the Global Positioning System: Results from the GPS/MET experiment, *Radio Sci.*, *33*, 175–190.

Hierro, R., H. Pessano, P. Llamedo, A. de la Torre, P. Alexander, and A. Odiard (2013), Orographic effects related to deep convection events over the Andes region, *Atmos. Res.*, *120–121*, 216–225, doi:10.1016/j.atmosres.2012.08.020.

Hines, C. O. (1960), Internal atmospheric gravity waves at ionospheric heights, *Can. J. Phys.*, *38*, 1441–1481.

Jakowski, N., A. Wehrenpfennig, S. Heise, C. Reigber, H. Lühr, L. Grunwaldt, and T. K. Meehan (2002), GPS radio occultation measurements of the ionosphere from CHAMP: Early results, *Geophys. Res. Lett.*, *29*(10), 1457, doi:10.1029/2001GL014364.

Kursinski, E. R., G. A. Hajj, J. T. Schofield, R. P. Linfield, and K. R. Hardy (1997), Observing Earth's atmosphere with radio occultation measurements using the Global Positioning System, *J. Geophys. Res.*, *102*, 23,429–23,465.

Martinis, C. R., J. Baumgardner, S. M. Smith, M. Colerico, and M. Mendillo (2006), Imaging science at El Leoncito, Argentina, *Ann. Geophys.*, *24*, 1–12.

Melbourne, W. G., et al. (1994), The application of spacebourne GPS to atmospheric limb sounding and global change monitoring, Publ. 94–18, Jet Propulsion Laboratory.

Miró Amarante, G., M. Cueto Santamaría, M. Mosert, and R. G. Ezquer (2004), Day-to-day changes in experimental electron density profiles and their implications to IRI model, *Adv. Space Res.*, *34*, 1878–1886.

Miyoshi, Y., and H. Fujiwara (2009), Gravity waves in the equatorial thermosphere and their relation to lower atmospheric variability, *Earth Planets Space*, *61*, 471–478.

Nicolls, M. J., M. C. Kelley, A. J. Coster, S. A. Gonzalez, and J. J. Makela (2004), Imaging the structure of a large-scale TID using ISR and TEC data, *Geophys. Res. Lett.*, *31*,L09812, doi:10.1029/2004GL019797.

Oliver, W. L., Y. Otsuka, M. Sato, T. Takami, and S. Fukao (1997), A climatology of *F* region gravity wave propagation over the middle and upper atmosphere radar, *J. Geophys. Res.*, *102*, 14,499–14,512.

Scheer, J., and E. R. Reisin (2010), Statistical properties of nonlinear wave signatures in OH and O_2 airglow brightness data observed at lower midlatitudes, *J. Atmos. Sol. Terr. Phys.*, *72*, 588–594.

Schmidt, T., A. de la Torre, and J. Wickert (2008), Global gravity wave activity in the tropopause region from CHAMP radio occultation data, *Geophys. Res. Lett.*, *35*, L16807, doi:10.1029/2008GL034986.

Smith, S., J. Baumgardner, and M. Mendillo (2009), Evidence of mesospheric gravity-waves generated by orographic forcing in the troposphere, *Geophys. Res. Lett.*, *36*, L08807, doi:10.1029/2008GL036936.

Testud, J. (1972), Interactions between gravity waves and ionization in the ionosphere *F* region, *Space Res.*, *XII*, 1163–1178.

Tsai, L.-C., W. H. Tsai, W. S. Schreiner, F. T. Berkey, and J. Y. Liu (2001), Comparisons of GPS/MET retrieved ionospheric electron density and ground based ionosonde data, *Earth Planets Space*, *53*, 193–205.

Vadas, S. L. (2013), Compressible *f*-plane solutions to body forces, heatings, and coolings, and application to the primary and secondary gravity waves generated by a deep convective plume, *J. Geophys. Res. Space Physics*, *118*, 2377–2397, doi:10.1002/jgra.50163.

Wickert, J., et al. (2009), GPS radio occultation: Results from CHAMP, GRACE and FORMOSAT-3/COSMIC, *Terr. Atmos. Oceanic Sci.*, *20*(1), 35–50, doi:10.3319/TAO.2007.12.26.01(F3C).

Yeh, K. C., and C. H. Liu (1974), Acoustic-gravity waves in the upper atmosphere, *Rev. Geophys. Space Phys.*, *12*, 193–216.